An accurate measurement of the sea-level muon spectrum within the range 4 to 3000 GeV/c

B C Rastin

Department of Physics, University of Nottingham, Nottingham NG7 2RD, UK

Abstract. The differential and integral spectra of muons moving in the near-vertical direction have been measured at Nottingham using a solid iron magnet spectrometer. This instrument utilised an automatic recording system for data collection which allowed the range of muon momenta covered by this investigation to extend from 4 to 3000 GeV/c, the lower limit being set by the magnet itself.

The diffusion model for particle propagation through the Earth's atmosphere was used to provide the muon momentum spectrum incident upon the instrument. A comparison of this spectrum, after modification by scattering and errors in the determination of the angular deflection, with the measured spectrum allowed a value of -2.72 ± 0.01 to be assigned to the exponent of the primary spectrum. If a contribution to the sea-level muon flux from the decay of K mesons is included then better agreement between the theoretical and experimental spectra is obtained for a value of the exponent of -2.73 together with a K/π ratio at production of 0.087. However, when the muon momentum range is reduced to 28–3000 GeV/c the comparison between the measured and the theoretical spectra shows agreement for an exponent of -2.60 ± 0.01 for 100% π-meson parentage. Further, the inclusion of K-meson decay in this case is inconclusive since it does not allow any sensible values to be assigned to the exponent or the contribution provided by this process.

1. Introduction

The measurements to be reported were carried out using the Nottingham cosmic-ray spectrometer. The data obtained from the original instrument, which had a maximum detectable momentum (MDM) of 360 GeV/c, have been summarised in a previous paper (Appleton *et al* 1971, hereafter referred to as I). The MDM of the present spectrometer has been increased to 3.40 TeV/c by increasing the separation between the detectors as well as the number of layers of flash tubes in each of the arrays. To facilitate the collection and processing of the data an automatic recording system based on video techniques (Harrison and Rastin 1969, hereafter referred to as II) was incorporated into the apparatus. This spectrometer is situated at an altitude of 170′ above sea level with an associated latitude and longitude of 52° 57′ N and 1° 12′ W. The spectrum obtained from this investigation is compared with the results from other workers and is used in conjunction with the diffusion model of particle propagation through the atmosphere to infer the exponent of the primary cosmic-ray beam. The contribution to the muon intensity at sea level from the decay of both π and K mesons has also been determined on the basis of this theoretical treatment.

2. The spectrometer

A scale diagram of the spectrometer is shown in figure 1 and a summary of the main features of the instrument is given in table 1. This spectrometer utilises a four-fold coincidence between the scintillation counters A, B, C and D to register the passage of a charged particle through the apparatus. The trajectory of this particle is delineated by four arrays each containing eight layers of neon flash tubes situated at levels FT1, FT2, FT3 and FT4. The solid iron magnet shown has been described previously (Cousins *et al* 1969, Bull *et al* 1965a) and for completeness a summary of the more important parameters is included in table 1. The average magnetic induction in the wound arm for an operating current of 16 A is 17.5 kG and this is uniform to better than ±1% at this level of magnetising current. The root-mean-square error in the location of both the incident and emergent trajectories each defined by two flash-tube arrays is $(0.167 \pm 0.003) \times 10^{-3}$ rad (see Bull *et al* 1962b); hence the MDM of the instrument is (3.40 ± 0.09) TeV/c.

The equations which describe the trajectory of the particle within the magnetic field have been derived previously by Bull *et al* (1965a) and are based in the main on the assumption that the rate of loss of energy per unit path length is constant. These equations
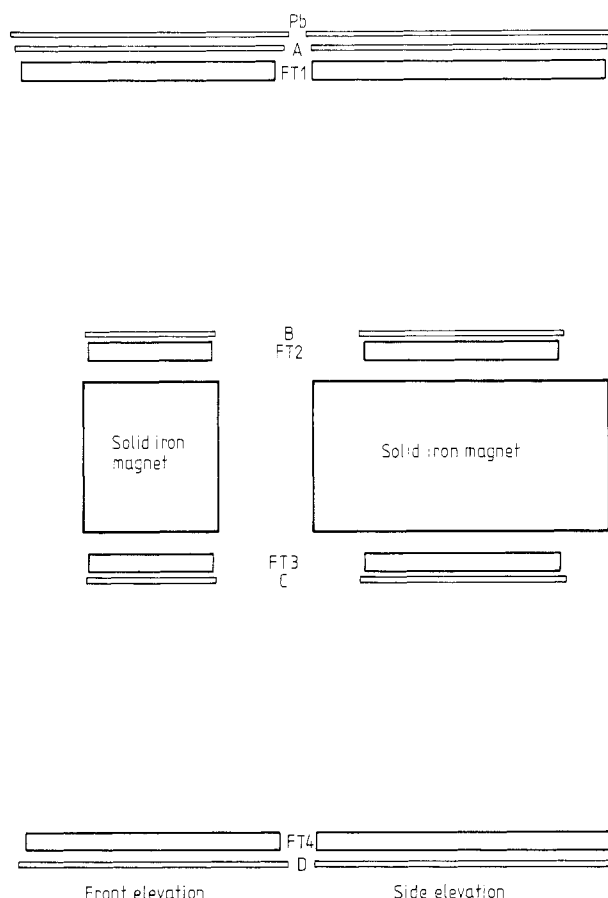

Figure 1. Nottingham cosmic-ray spectrometer: A, B, C and D, scintillators; FT1, FT2, FT3 and FT4, flash-tube arrays; Pb, lead absorber.

Table 1. Parameters of the spectrometer.

Flash-tube array data	
Internal diameter of the flash tubes	0.59 cm
External diameter of the flash tubes	0.79 cm
Horizontal separation (centre to centre)	0.84 cm
Vertical separation (centre to centre)	2.0 cm
Sensitive area of flash tubes used in FT1 and FT4	94 cm × 109 cm
Sensitive area of flash tubes used in FT2 and FT3	45 cm × 76 cm
Number of layers of flash tubes in each array	8
Separation between the centre of gravity of the arrays above or below the magnetic field	309 cm
RMS error associated with the incident and emergent trajectories	$(0.167 \pm 0.003) \times 10^{-3}$ rad

Solid iron magnet data	
Useful magnetic volume	51 cm × 102 cm × 153 cm
Energising current	16 A
Power dissipation	3 kW
Magnetic induction (wound arm)	17.5 ± 0.2 kG
Uniformity across plate	1.2%
Uniformity through magnet	± 1%
Magnetic induction (unwound arm)	17.0 ± 0.2 kG
Uniformity across plate	0.4%
Uniformity through magnet	± 1%
Field line integral (wound arm)	$(2.68 \pm 0.03) \times 10^6$ G cm

Maximum detectable momentum	(3.40 ± 0.09) TeV/c
Geometrical acceptance solid angle	36.05 cm^2 sr

can be written in the form

$$p_i = \frac{LK[1 + (\varepsilon^2/K^2)]}{I(\psi_1) - I(\psi_2)} \tag{1}$$

where

$$I(\psi) = \exp\left(\frac{S\varepsilon}{K}(\psi_1 - \psi)\right)\left(\cos\psi + \frac{S\varepsilon}{K}\sin\psi\right)$$

and

$$x = \frac{p_i}{K[1 + (\varepsilon^2/K^2)]}(I'(\psi_2) - I'(\psi_1)) \tag{2}$$

where

$$I'(\psi) = \exp\left(\frac{S\varepsilon}{K}(\psi_1 - \psi)\right)\left(\sin\psi - \frac{S\varepsilon}{K}\cos\psi\right);$$

ε is the momentum loss per centimetre, K is 300 times the magnetic induction (wound arm), $S = +1$ if $\psi_1 < \psi_2$ or -1 if $\psi_1 > \psi_2$ and the remaining symbols are defined in figure 2.

In this treatment the effect of multiple scattering within the iron has been ignored and
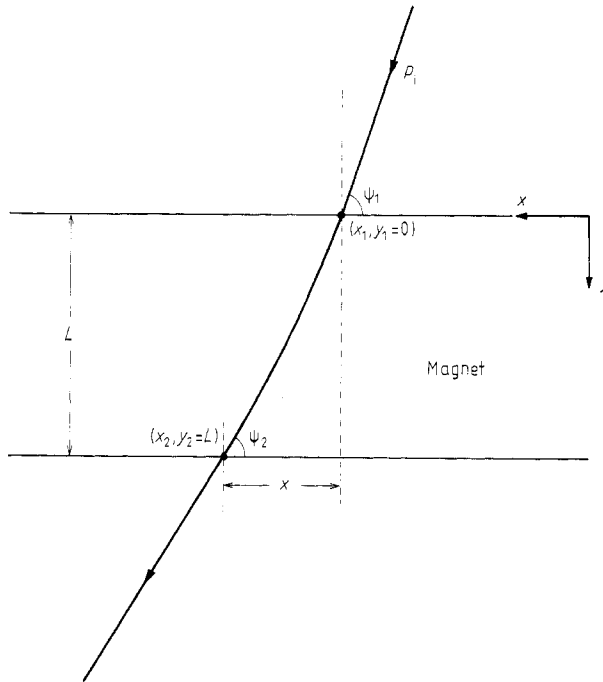
Figure 2. Trajectory of a charged particle through the solid iron magnet.

hence x and ψ_2 included in equations (1) and (2) cannot be measured directly. The information provided by the flash-tube arrays allows the x intercepts on the upper and lower surfaces of the magnet (x_1, x_2') and the incident and emergent angles (ψ_1, ψ_2') to be determined. This enables an approximate value for the incident momentum to be found using equation (1), and hence the associated point of emergence x_2 can be computed. The difference between this x_2 and the observed point x_2' is a measure of the validity of the particle since the difference between these two parameters should be less than $\pm 3\sigma_p$, where σ_p is the standard deviation of the lateral scattering distribution for a particle of this momentum (Eyges 1948) in the majority of cases. This forms the basis of one of the selection criteria used in this investigation to reduce the probability of collecting spurious data, for example low-energy particles being mistaken for particles of high energy due to scattering or the simultaneous passage of two particles through the instrument, one through the top two flash-tube arrays and the second through the bottom two arrays.

   The electronic circuitry associated with the operation of the scintillation counters and flash-tube detectors is in common use and hence is summarised adequately by the schematic diagram given in figure 3. A block diagram of the data-handling system produced at Nottingham to operate in conjunction with the spectrometer is shown in figure 4 and detailed descriptions of the main elements used in this system have been given in II. The flash-tube data obtained from the digitising system were analysed using the method developed by Bull *et al* (1962a) and this allows two further selection criteria to be implemented. These are associated with (*a*) a very low probability of producing the observed pattern of flashed tubes and (*b*) the most probable trajectory of the particle being outside the sensitive region as defined by the dimensions of the scintillation counters.

   Events which fail one or more of the three selection criteria mentioned above are rejected. However, the stringent application of these methods of selection can cause some
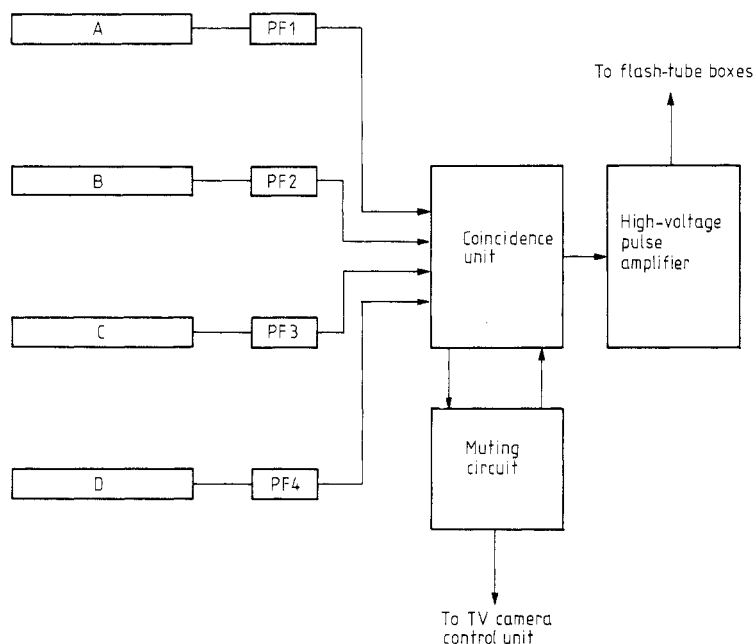
Figure 3. Block diagram of the electronics: A, B, C and D, scintillators; PF1, PF2, PF3 and PF4, pulse-forming units.

valid events to be rejected. Without the expenditure of a prohibitive amount of effort to provide very detailed monitoring of each experimental run these measurements cannot be claimed to represent absolute intensities and a suitable normalisation procedure was adopted. This involved normalisation to a measured muon absolute intensity at a muon momentum within the range covered by the spectrometer. Such information has been provided by Barbouti and Rastin (1983) using an instrument specifically designed to measure absolute muon intensities under a range of known absorber thicknesses.

To determine the geometrical acceptance solid angle for the spectrometer the top scintillation counter (A) was divided into small areas Δx in the front elevation and Δy in the side elevation. The limits for the acceptance of particles of infinite momentum subtended at each of these small areas as defined by the three remaining scintillation counters and the volume of the magnetic material were determined. Hence the total geometrical solid angle could be computed for the values of Δx and Δy chosen. The sizes of the increments were decreased and a new geometrical solid angle was obtained. This procedure was repeated until the asymptote which the computed solid angle approached was defined to better than 1%.

3. The correction factors

The acceptance solid angle as defined above applies to particles of infinite momentum and as such does not include any factors to account for the effects of Coulomb scattering or magnetic deflection on the probability of a particle being accepted. To correct for these effects it was convenient to consider each of them separately.
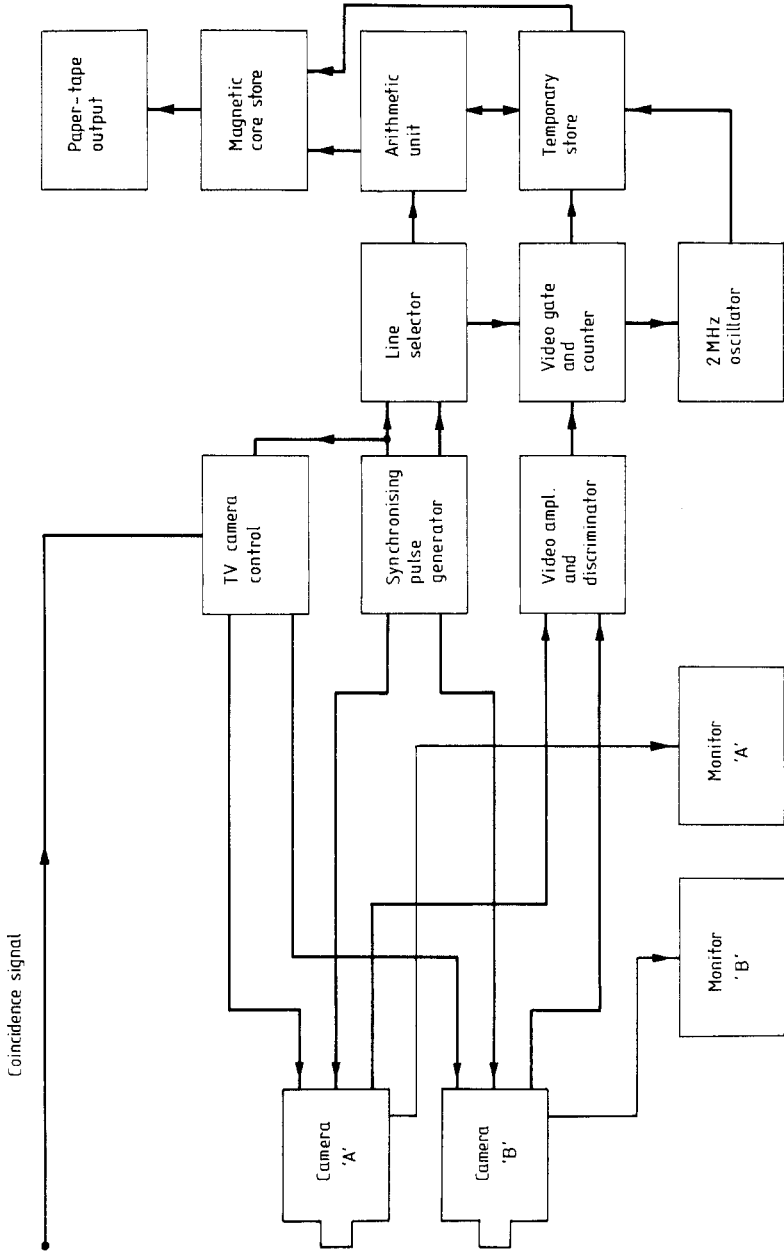
Figure 4. Schematic diagram of data handling system.

3.1. Coulomb scattering

The method used to evaluate the correction factor for a muon with any given momentum at incidence involved the simulation of trajectories through the instrument considering the front and side elevations separately. The expression for the standard deviation of the angular scattering distribution was taken from the work of Eyges (1948) and included the modifications suggested by Crookes and Rastin (1973). The acceptance probability for the given momentum depended upon the points of incidence of the trajectories as well as the inclination of these trajectories to the axis of the instrument. In practice muons were incident at all points on the surface of the top scintillation counter and at all angles. It was impossible to simulate such conditions exactly and hence trajectories with discrete spatial and angular increments were considered. The sizes of these increments were decreased and the calculated acceptance probability approached the true probability asymptotically. The procedure was continued until the accuracy of the final calculated acceptance probability was better than 1%. The variation of the muon intensity with zenith angle was taken to be adequately represented by the $(cosine)^2$ distribution and the effect of lateral scattering on the incident particle was neglected. The overall acceptance probability obtained using this technique is given in table 2.

Table 2. Acceptance functions for the spectrometer.

Incident momentum (GeV/c)	Probability of muon being accepted		Overall acceptance probability
	Coulomb scattering	Magnetic deflection	
3	0.571	0	0
3.5	0.746	0	0
4	0.832	0	0
4.5	0.880	0.04	0.352
5	0.909	0.233	0.212
5.5	0.929	0.351	0.326
6	0.945	0.449	0.424
6.5	0.955	0.529	0.505
7	0.962	0.598	0.575
7.5	0.968	0.649	0.628
8	0.973	0.691	0.672
8.5	0.976	0.727	0.710
9	0.979	0.757	0.741
9.5	0.983	0.781	0.768
10	0.985	0.804	0.792
12	0.989	0.863	0.854
15	0.993	0.909	0.903
20	0.995	0.952	0.947
25	0.997	0.969	0.966
30	0.998	0.980	0.978
35	0.999	0.983	0.982
40	1.000	0.990	0.990
50	1.000	0.995	0.995
60	1.000	0.997	0.997
∞	1.000	1.000	1.000

3.2. Magnetic deflection

In this case the trajectories of the muons incident on the top surface of the magnet were simulated using the method outlined above. The path of each particle was traced through the solid iron magnet at intervals of 10 g cm^{-2} using equations (1) and (2). The acceptance conditions were such that at no interval did the trajectory lie outside the solid iron magnet and the incident and emergent paths of the particle passed through the scintillation counters giving the required coincidence. The correction factor derived in this manner to describe the effect of the loss of particles by the deflection in the magnetic field is given in table 2 together with the overall acceptance probability for the spectrometer due to the combined effects of both the processes mentioned above.

4. Experimental results

4.1. The zero-field characteristic of the spectrometer

The angular deflection distribution obtained with the magnet in the unmagnetised state is a result of the effect of Coulomb scattering of the particle in the material of the spectrometer and the errors in the determination of the angles of incidence and emergence associated with the flash-tube arrays. In this type of spectrometer the majority of the scattering material is located centrally in the form of the solid iron magnet, the dimensions and chemical composition of which are known precisely. Consequently an angular scattering distribution can be predicted which includes the effects of scattering in the magnetic material as well as angular errors inherent in measurements made using the flash-tube arrays. Hence by comparing the experimental and theoretical distributions it is possible to obtain information on the scattering in the detectors, the errors in the angular measurements and the alignment of the flash-tube boxes. To this end 7339 single-particle traversals of the instrument were recorded and arranged in 0.01 rad deflection categories; the resulting distribution is shown by the broken lines in figure 5. The predicted distribution obtained by simulating the trajectories of particles using the method outlined in § 3.1 and normalised to the observed number of single-particle traversals is also included in figure 5. The muon momentum range covered in this procedure extended from 2.4 to 100 GeV/c and the muon differential intensity was taken to vary according to (muon momentum)$^{-2.7}$. The observed and predicted distributions can be seen to agree within the limits of statistical uncertainty, the mean and standard deviation of the measurements being 0.0012 and 0.0614 rad as compared with 0 and 0.0615 rad for the theoretical distribution. It can therefore be concluded that the effect of scattering in the material of the spectrometer apart from the solid iron magnet itself is small. Further, the observed distribution shows no gross lack of symmetry between negative and positive deflections and the mean of the measured distribution is consistent with a population mean of zero. Hence it can also be claimed that no serious misalignment of the flash-tube boxes exists and the errors associated with the angular measurements have been estimated accurately.

4.2. Measurement of the muon deflection spectrum

The data obtained in this experiment were collected during the period September 1974 to May 1978 and represented 364 623 events acceptable as single-particle traversals of the instrument. The magnetic field was reversed at weekly intervals so that approximately the
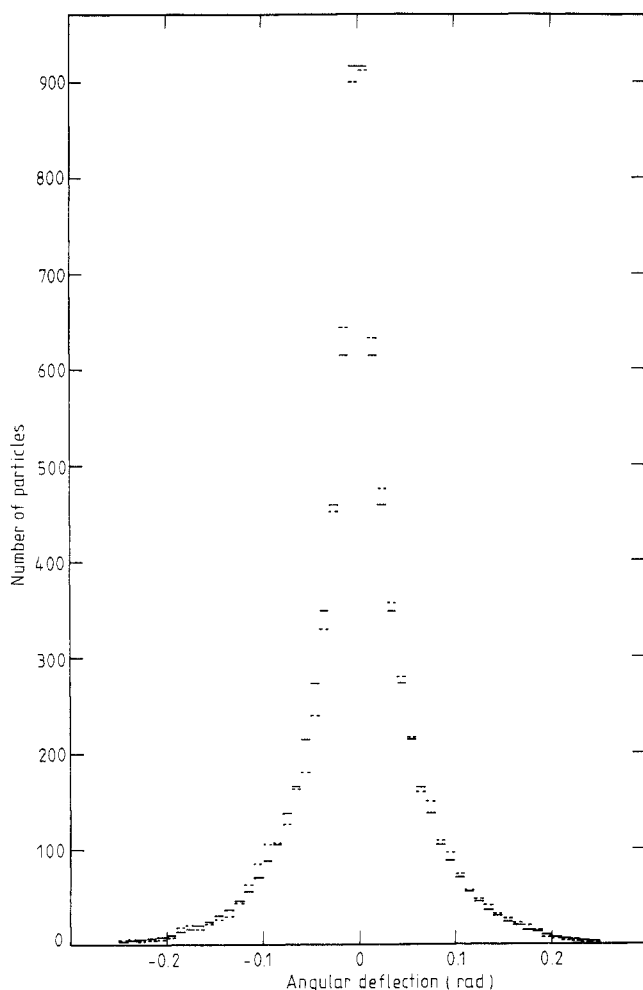
Figure 5. Comparison of the observed (– – –) and predicted (———) scattering distributions.

same numbers of events were accepted for both field directions to avoid the introduction of any possible instrumental bias. The knowledge of the direction of the applied magnetic field enabled the data to be collated and arranged in angular intervals of width 0.01 rad, producing the deflection spectrum given in table 4. In order to facilitate the investigation of the high momentum range of the muon spectrum the top three categories were further sub-divided into angular intervals of width 0.001 rad and this information is shown in table 5.

5. Determination of the sea-level muon momentum spectrum

The deflection spectrum obtained in § 4.2 is the result of the convolution of the true sea-level muon deflection spectrum with functions which describe (a) the magnetic deflection and Coulomb scattering in and out of the acceptance solid angle, (b) multiple scattering within the magnet, which affects the estimate of the angular deflection of the accepted events, and (c) errors in the angular measurements which are inherent in the detectors used.

Since the functions which represent the processes (a), (b) and (c) are known, the deconvolution of the measured spectrum could be used to yield the true sea-level spectrum. It is more convenient, however, to adopt a sea-level spectrum derived theoretically and modify this spectrum for the effects of (a), (b) and (c). The resulting deflection spectrum is then compared with the measured spectrum by means of the χ^2 test and the parameters associated with the theoretical spectrum are altered until the 'best fit' is obtained. The theoretical spectrum corresponding to the best-fit case is then taken to be the sea-level muon spectrum as given by these results.

The diffusion model of particle propagation through the Earth's atmosphere has been used to provide the theoretical spectrum in this investigation. The modification suggested by Smith and Duller (1959) has been included and the resulting expression for the differential muon momentum spectrum produced from π-meson parents is

$$D(E_\mu) = A P_\mu E_\pi^{-\gamma} \frac{b j_\pi}{(E_\pi + b j_\pi)} \tag{3}$$

where A is a constant which can be determined by normalisation to a measured muon absolute intensity and P_μ is the probability that a muon, produced at a depth x g cm^{-2} from the top of the atmosphere with a momentum $p_\mu(x)$, survives to sea level (x_0) (Rossi 1952). In the derivation of P_μ it is assumed that the muons are produced at a depth of 100 g cm^{-2}, E_π is the energy of a π meson at a depth x which would give rise to a muon of energy E_μ at sea level and hence $E_\pi r_\pi = E_\mu + \varepsilon(x_0 - x)$, γ is the exponent of the primary spectrum and the definitions of the remaining symbols as well as the values for the constants used in the determination of the muon spectra are given in table 3.

Table 3. Constants used in derivation of the comparison spectra.

Depth of the atmosphere (x_0)	1033 g cm^{-2}
Gas constant (R)	8.314 J K^{-1} g^{-1} mol^{-1}
Effective temperature of the atmosphere (T_e)	219 K
Effective molecular weight of air (M)	28.966
Acceleration due to gravity at 53° N (g)	981.3 cm s^{-2}
Density of air at sea level at 10 °C and 76 cm Hg $(\rho(x_0))$	0.00124 g cm^{-3}
Velocity of light (c)	3 × 10^{10} cm s^{-1}
Rate of energy loss in air (ε)	2.225 MeV g^{-1} cm^{-2}
Energy equivalent of the rest mass of the muon $(m_\mu c^2)$	105.659 MeV
Energy equivalent of the rest mass of the pion $(m_\pi c^2)$	139.580 MeV
Energy equivalent of the rest mass of the kaon $(m_K c^2)$	493.80 MeV
Mean lifetime of muon at rest $(\tau_{\mu 0})$	2.20 × 10^{-6} s
Mean lifetime of pion at rest $(\tau_{\pi 0})$	2.616 × 10^{-8} s
Mean lifetime of kaon at rest (τ_{K_0})	1.240 × 10^{-8} s
Depth of production of muons	100 g cm^{-2}
Correction factor to improve approximation caused by assuming an isothermal atmosphere (b)	0.7689
Ratio of energies of daughter to parent for decay of pion $(r_\pi = (m_\pi^2 + m_\mu^2)/2m_\pi^2)$	0.7865
Ratio of energies of daughter to parent for decay of kaon $(r_K = (m_K^2 + m_\mu^2)/2m_K^2)$	0.5229
Absorption mean free path for protons, pions and kaons (λ)	120 g cm^{-2}
$j_\pi = m_\pi x_0 c/\rho(x_0)\tau_{\pi 0}$	148.16 GeV
$j_K = m_K x_0 c/\rho(x_0)\tau_{K_0}$	1105.8 GeV

Deflection spectra corrected for the effects mentioned above ((a), (b) and (c)) have been derived for various values of the primary exponent γ. The application of the χ^2 test shows that the experimental data given in table 4 can be best represented by a spectrum with $\gamma = 2.72 \pm 0.008$, which corresponds to the 25% level of significance. To increase the sensitivity of the test to the data from the high momentum range this procedure has been repeated for the cumulative data and a best-fit exponent of -2.72 ± 0.004 was obtained with an associated level of significance of 48%. The errors shown above have been quoted at the 5% level of significance following the procedure suggested by Lampton *et al* (1976). The experimental and theoretical data together with the lower and average momentum of each category are shown in table 4. Also included in this table are the 'experimental points' obtained by multiplying the theoretical value of the muon intensity, normalised at a muon momentum of 5 GeV/c to an integral intensity of 2.26×10^{-3} cm^{-2} sr^{-1} s^{-1} (Barbouti and Rastin 1983), by the ratio of the number of muons observed in a given category to the number predicted. The errors which have been given are purely statistical and correspond to one standard deviation.

The diffusion model used above can easily be modified to include a contribution to the muon intensity at sea level from K-meson parents. In this case the expression for the differential muon intensity becomes

$$D(E_\mu) = A\left(\alpha P_\mu E_\pi^{-\gamma} \frac{bj_\pi}{E_\pi + bj_\pi} + (1-\alpha)P'_\mu E_K^{-\gamma} \frac{bj_K}{E_K + bj_K}\right) \qquad (4)$$

where α and $(1-\alpha)$ determine the contributions to the sea-level muon flux from π-meson and K-meson parents. Deflection spectra based on this equation were determined for various values of γ with different values of α using the method outlined above. The use of the χ^2 test in this case shows that the data given in table 4 as well as the cumulative data can be represented by a sea-level spectrum with an exponent of -2.73 for $\alpha = 0.85$; the associated levels of significance are 36% and 75% respectively. If the 5% level is again taken as a suitable value at which to quote the errors then the integral spectrum gives $\gamma = 2.73^{+0.03(\alpha=0.55)}_{-0.02(\alpha=1)}$.

To facilitate the investigation of the high-energy region of the muon spectrum at sea level the data contained in the angular categories $0-3 \times 10^{-2}$ rad were re-analysed and distributed over 30 cells each of width 1×10^{-3} rad. This is shown in table 5 together with the minimum and average momentum of each of the categories. Comparison deflection spectra were derived using the diffusion model of particle propagation through the Earth's atmosphere for values of the exponent γ from 2.50 to 2.75 on the assumption of 100% π-meson parentage. These spectra, modified for the effects (a), (b) and (c) mentioned above, were compared with the experimental data using the χ^2 test. The minimum value of χ^2 occurred for $\gamma = 2.60$ at a 77% level of significance. This procedure was repeated for the cumulative data and the same value for the best-fit exponent was obtained with a 25% level of significance. If the 5% significance level is again taken as the level to quote errors then $\gamma = 2.60 \pm 0.03$ while for the cumulative data $\gamma = 2.60 \pm 0.01$. The number of particles in each of the categories predicted using this model together with the 'experimental points' obtained using the method mentioned above have also been included in table 5.

The 'experimental points' given in tables 4 and 5 as well as the data for the very low momentum region presented by Barbouti and Rastin (1983) have been plotted in figure 6. The best-fit curves shown in this figure are composites of the best-fit spectra for the momentum ranges 0.35–10, 4–100 and 29–1000 GeV/c derived from the two experiments.

Table 4.

Deflection interval (rad)	Total number of particles observed	Number of particles predicted	Minimum momentum of category (GeV/c)	Average momentum of category (GeV/c)	'Experimental points' normalised† to an integral intensity of 2.26×10^{-3} cm^{-2} sr^{-1} s^{-1} at a muon momentum of 5 GeV/c‡	
					Differential (cm^{-2} sr^{-1} s^{-1} (GeV/c)$^{-1}$)	Integral (cm^{-2} sr^{-1} s^{-1})
0–0.01	5296	5280	81.22	136.55	$(9.6 \pm 0.1) \times 10^{-8}$	$(1.81 \pm 0.02) \times 10^{-5}$
0.01–0.02	14973	14977	41.23	54.55	$(1.66 \pm 0.01) \times 10^{-6}$	$(7.62 \pm 0.05) \times 10^{-5}$
0.02–0.03	20733	20474	27.90	33.31	$(6.89 \pm 0.04) \times 10^{-6}$	$(1.64 \pm 0.01) \times 10^{-4}$
0.03–0.04	24436	24244	21.24	24.14	$(1.63 \pm 0.01) \times 10^{-5}$	$(2.70 \pm 0.01) \times 10^{-4}$
0.04–0.05	26137	26174	17.25	19.05	$(2.97 \pm 0.02) \times 10^{-5}$	$(3.87 \pm 0.01) \times 10^{-4}$
0.05–0.06	26391	26485	14.59	15.81	$(4.70 \pm 0.03) \times 10^{-5}$	$(5.11 \pm 0.01) \times 10^{-4}$
0.06–0.07	25814	26044	12.69	13.58	$(6.72 \pm 0.04) \times 10^{-5}$	$(6.37 \pm 0.02) \times 10^{-4}$
0.07–0.08	24949	25163	11.27	11.94	$(9.05 \pm 0.06) \times 10^{-5}$	$(7.65 \pm 0.02) \times 10^{-4}$
0.08–0.09	23522	23787	10.16	10.69	$(1.156 \pm 0.008) \times 10^{-4}$	$(8.92 \pm 0.02) \times 10^{-4}$
0.09–0.10	21984	22225	9.28	9.70	$(1.43 \pm 0.01) \times 10^{-4}$	$(1.020 \pm 0.002) \times 10^{-3}$
0.10–0.11	20183	20354	8.56	8.91	$(1.71 \pm 0.01) \times 10^{-4}$	$(1.140 \pm 0.002) \times 10^{-3}$
0.11–0.12	18533	18582	7.96	8.25	$(2.02 \pm 0.01) \times 10^{-4}$	$(1.260 \pm 0.003) \times 10^{-3}$
0.12–0.13	16659	16744	7.46	7.70	$(2.32 \pm 0.02) \times 10^{-4}$	$(1.377 \pm 0.003) \times 10^{-3}$

0.13–0.14	14903	14938	7.03	7.24	$(2.63 \pm 0.02) \times 10^{-4}$	$(1.489 \pm 0.003) \times 10^{-3}$
0.14–0.15	13282	13224	6.65	6.84	$(2.95 \pm 0.03) \times 10^{-4}$	$(1.599 \pm 0.003) \times 10^{-3}$
0.15–0.16	11744	11551	6.33	6.49	$(3.30 \pm 0.03) \times 10^{-4}$	$(1.705 \pm 0.003) \times 10^{-3}$
0.16–0.17	10210	10106	6.04	6.18	$(3.59 \pm 0.04) \times 10^{-4}$	$(1.807 \pm 0.003) \times 10^{-3}$
0.17–0.18	8759	8601	5.79	5.91	$(3.92 \pm 0.04) \times 10^{-4}$	$(1.905 \pm 0.003) \times 10^{-3}$
0.18–0.19	7439	7352	5.56	5.67	$(4.19 \pm 0.05) \times 10^{-4}$	$(2.000 \pm 0.003) \times 10^{-3}$
0.19–0.20	6259	6139	5.36	5.46	$(4.52 \pm 0.06) \times 10^{-4}$	$(2.090 \pm 0.004) \times 10^{-3}$
0.20–0.21	5226	5153	5.18	5.27	$(4.79 \pm 0.07) \times 10^{-4}$	$(2.176 \pm 0.004) \times 10^{-3}$
0.21–0.22	4260	4212	5.01	5.09	$(5.05 \pm 0.08) \times 10^{-4}$	$(2.259 \pm 0.004) \times 10^{-3}$
0.22–0.23	3449	3367	4.86	4.93	$(5.40 \pm 0.09) \times 10^{-4}$	$(2.339 \pm 0.004) \times 10^{-3}$
0.23–0.24	2734	2684	4.72	4.79	$(5.6 \pm 0.1) \times 10^{-4}$	$(2.415 \pm 0.004) \times 10^{-3}$
0.24–0.25	2044	2094	4.60	4.66	$(5.7 \pm 0.1) \times 10^{-4}$	$(2.487 \pm 0.004) \times 10^{-3}$
0.25–0.26	1620	1593	4.48	4.54	$(6.14 \pm 0.2) \times 10^{-4}$	$(2.557 \pm 0.004) \times 10^{-3}$
0.26–0.27	1193	1186	4.37	4.43	$(6.31 \pm 0.2) \times 10^{-4}$	$(2.624 \pm 0.004) \times 10^{-3}$
0.27–0.28	844	853	4.28	4.32	$(6.4 \pm 0.2) \times 10^{-4}$	$(2.688 \pm 0.004) \times 10^{-3}$
0.28–0.29	614	607	4.19	4.23	$(6.8 \pm 0.3) \times 10^{-4}$	$(2.749 \pm 0.005) \times 10^{-3}$
0.29–0.30	433	430	4.10	4.14	$(7.0 \pm 0.3) \times 10^{-4}$	$(2.808 \pm 0.005) \times 10^{-3}$

† This normalisation procedure yielded a value of 0.319 for the parmeter A in equation (3).
‡ Barbouti and Rastin (1983).

Table 5.

Deflection interval (rad)	Total number of particles observed	Number of particles predicted	Minimum momentum of category (GeV/c)	Average momentum of category (GeV/c)	'Experimental points' normalised to an integral intensity of 1.64×10^{-4} cm^{-2} sr^{-1} s^{-1} at a muon momentum of 27.90 GeV/c	
					Differential (cm^{-2} sr^{-1} s^{-1} (GeV/c)$^{-1}$)	Integral (cm^{-2} sr^{-1} s^{-1})
0–0.001	62	58	801.31	1288.74	$(5.9 \pm 0.8) \times 10^{-11}$	$(1.0 \pm 0.1) \times 10^{-7}$
0.001–0.002	144	128	401.26	525.82	$(1.4 \pm 0.1) \times 10^{-9}$	$(5.7 \pm 0.4) \times 10^{-7}$
0.002–0.003	257	236	267.91	319.72	$(7.5 \pm 0.5) \times 10^{-9}$	$(1.51 \pm 0.07) \times 10^{-6}$
0.003–0.004	382	356	201.24	229.36	$(2.2 \pm 0.1) \times 10^{-8}$	$(2.9 \pm 0.1) \times 10^{-6}$
0.004–0.005	497	477	161.23	178.85	$(4.8 \pm 0.2) \times 10^{-8}$	$(4.8 \pm 0.1) \times 10^{-6}$
0.005–0.006	608	600	134.56	146.62	$(8.8 \pm 0.4) \times 10^{-8}$	$(7.2 \pm 0.2) \times 10^{-6}$
0.006–0.007	691	715	115.51	124.27	$(1.42 \pm 0.05) \times 10^{-7}$	$(9.8 \pm 0.2) \times 10^{-6}$
0.007–0.008	775	832	101.23	107.88	$(2.12 \pm 0.08) \times 10^{-7}$	$(1.28 \pm 0.02) \times 10^{-5}$
0.008–0.009	885	932	90.11	95.34	$(3.2 \pm 0.1) \times 10^{-7}$	$(1.63 \pm 0.02) \times 10^{-5}$
0.009–0.010	995	1042	81.22	85.43	$(4.4 \pm 0.1) \times 10^{-7}$	$(2.02 \pm 0.03) \times 10^{-5}$
0.010–0.011	1163	1140	73.95	77.42	$(6.3 \pm 0.2) \times 10^{-7}$	$(2.47 \pm 0.03) \times 10^{-5}$
0.011–0.012	1251	1226	67.79	70.80	$(7.6 \pm 0.2) \times 10^{-7}$	$(2.96 \pm 0.03) \times 10^{-5}$

|					
0.012–0.013	1298	62.76	65.23	$(1.04 \pm 0.03) \times 10^{-6}$	$(3.47 \pm 0.04) \times 10^{-5}$
0.013–0.014	1407	58.37	60.49	$(1.25 \pm 0.03) \times 10^{-6}$	$(4.03 \pm 0.04) \times 10^{-5}$
0.014–0.015	1448	54.56	56.40	$(1.56 \pm 0.04) \times 10^{-6}$	$(4.61 \pm 0.04) \times 10^{-5}$
0.015–0.016	1551	51.23	52.84	$(1.87 \pm 0.05) \times 10^{-6}$	$(5.23 \pm 0.05) \times 10^{-5}$
0.016–0.017	1630	48.28	49.71	$(2.23 \pm 0.06) \times 10^{-6}$	$(5.88 \pm 0.05) \times 10^{-5}$
0.017–0.018	1667	45.67	46.94	$(2.62 \pm 0.06) \times 10^{-6}$	$(6.55 \pm 0.05) \times 10^{-5}$
0.018–0.019	1741	43.33	44.47	$(3.03 \pm 0.07) \times 10^{-6}$	$(7.25 \pm 0.05) \times 10^{-5}$
0.019–0.020	1817	41.23	42.25	$(3.44 \pm 0.08) \times 10^{-6}$	$(7.97 \pm 0.06) \times 10^{-5}$
0.020–0.021	1820	39.32	40.25	$(3.91 \pm 0.09) \times 10^{-6}$	$(8.71 \pm 0.06) \times 10^{-5}$
0.021–0.022	1847	37.59	38.44	$(4.4 \pm 0.1) \times 10^{-6}$	$(9.45 \pm 0.06) \times 10^{-5}$
0.022–0.023	1958	36.01	36.79	$(5.1 \pm 0.1) \times 10^{-6}$	$(1.025 \pm 0.006) \times 10^{-4}$
0.023–0.024	2038	34.56	35.27	$(5.8 \pm 0.1) \times 10^{-6}$	$(1.108 \pm 0.007) \times 10^{-4}$
0.024–0.025	2093	33.23	33.88	$(6.3 \pm 0.1) \times 10^{-6}$	$(1.192 \pm 0.007) \times 10^{-4}$
0.025–0.026	2132	32.00	32.60	$(7.1 \pm 0.2) \times 10^{-6}$	$(1.278 \pm 0.007) \times 10^{-4}$
0.026–0.027	2133	30.90	31.42	$(7.8 \pm 0.2) \times 10^{-6}$	$(1.366 \pm 0.007) \times 10^{-4}$
0.027–0.028	2189	29.80	30.32	$(8.5 \pm 0.2) \times 10^{-6}$	$(1.455 \pm 0.008) \times 10^{-4}$
0.028–0.029	2231	28.82	29.30	$(9.3 \pm 0.2) \times 10^{-6}$	$(1.546 \pm 0.008) \times 10^{-4}$
0.029–0.030	2292	27.90	28.35	$(1.03 \pm 0.02) \times 10^{-5}$	$(1.640 \pm 0.008) \times 10^{-4}$
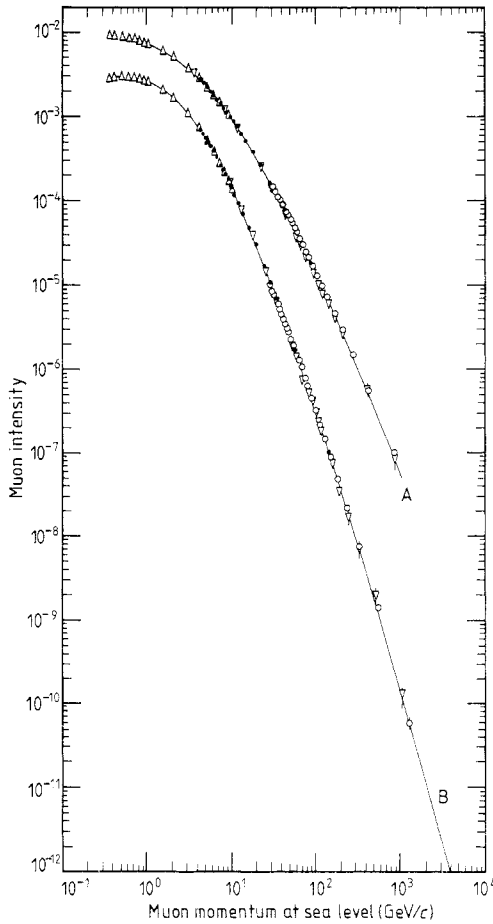
Figure 6. The differential (in $cm^{-2} sr^{-1} s^{-1}$ $(GeV/c)^{-1}$) and integral (in $cm^{-2} sr^{-1} s^{-1}$) muon spectra for the vertical direction measured at Nottingham: A, muon integral spectrum; B, muon differential spectrum; ●, present results for low momentum; O, present results for high momentum; △, Barbouti and Rastin (1983); ▽, Appleton *et al* (1971) normalised to a muon integral intensity of $2.26 \times 10^{-3} cm^{-2} sr^{-1} s^{-1}$ at $p_\mu = 5$ GeV/c; ——, best-fit spectra to the recent Nottingham data.

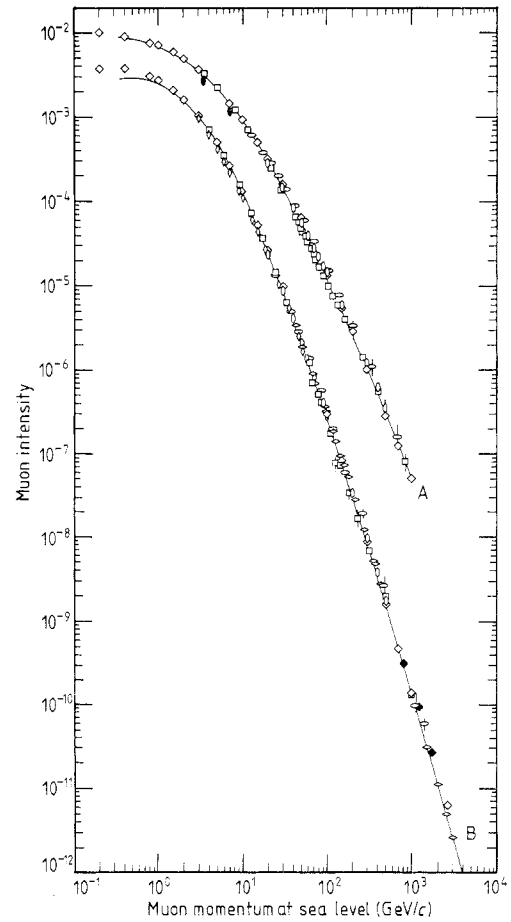**Figure 7.** Comparison of the present best-fit differential (in $cm^{-2} sr^{-1} s^{-1}$ $(GeV/c)^{-1}$) and integral (in $cm^{-2} sr^{-1} s^{-1}$) spectra with the data obtained by other workers: A, integral spectrum; B, differential spectrum; ——, present best-fit spectra; ◇, Allkofer *et al* (1971); ●, Ayre *et al* (1971); O, Ayre *et al* (1975); ◆, Thompson *et al* (1977); ◊, Bateman *et al* (1971); □, Appleton *et al* (1971) normalised to $2.26 \times 10^{-3} cm^{-2} sr^{-1} s^{-1}$ at $p_\mu = 5$ GeV/c; ○, Nandi and Sinha (1972); ◇, Komori (1977).

The integral and differential spectra for standard values of muon momentum taken from the best-fit curves are given in table 6.

The effect on the high-energy muon flux at sea level of a contribution from K-meson parents was investigated using the method outlined previously which involved deriving comparison spectra by means of equation (4) for values of γ in the range 2.50 to 2.70 and values of α from 0 to 1. No minimum in the χ^2 was observed for sensible values of α in this investigation; this showed clearly that an increase in γ could be compensated for by a suitable increase in the percentage of muons from K-meson parents. Further, the value of χ^2 decreased continuously using this procedure and hence no definite conclusions could be

Table 6. Best-fit muon differential and integral spectra at standard values of momentum.

Muon momentum (GeV/c)	Muon differential intensity (cm^{-2} sr^{-1} s^{-1} (GeV/c)$^{-1}$)	Muon integral intensity (cm^{-2} sr^{-1} s^{-1})
0.35	2.85×10^{-3}	9.13×10^{-3}
0.40	2.90×10^{-3}	8.98×10^{-3}
0.50	2.94×10^{-3}	8.69×10^{-3}
0.60	2.92×10^{-3}	8.40×10^{-3}
0.70	2.87×10^{-3}	8.11×10^{-3}
0.80	2.80×10^{-3}	7.83×10^{-3}
0.90	2.71×10^{-3}	7.55×10^{-3}
1.00	2.62×10^{-3}	7.29×10^{-3}
1.50	2.12×10^{-3}	6.10×10^{-3}
2.00	1.69×10^{-3}	5.16×10^{-3}
3.00	1.10×10^{-3}	3.80×10^{-3}
4.00	7.40×10^{-4}	2.90×10^{-3}
5.00	5.17×10^{-4}	2.27×10^{-3}
6.00	3.75×10^{-4}	1.83×10^{-3}
7.00	2.80×10^{-4}	1.51×10^{-3}
8.00	2.16×10^{-4}	1.25×10^{-3}
9.00	1.69×10^{-4}	1.06×10^{-3}
10.00	1.35×10^{-4}	9.05×10^{-4}
15.00	5.28×10^{-5}	4.79×10^{-4}
20.00	2.58×10^{-5}	2.93×10^{-4}
25.00	1.45×10^{-5}	1.96×10^{-4}
30.00	8.69×10^{-6}	1.40×10^{-4}
40.00	3.90×10^{-6}	8.23×10^{-5}
50.00	2.11×10^{-6}	5.35×10^{-5}
60.00	1.26×10^{-6}	3.72×10^{-5}
70.00	8.03×10^{-7}	2.72×10^{-5}
80.00	5.42×10^{-7}	2.06×10^{-5}
90.00	3.81×10^{-7}	1.60×10^{-5}
100.00	2.77×10^{-7}	1.28×10^{-5}
150.00	7.85×10^{-8}	5.18×10^{-6}
200.00	3.12×10^{-8}	2.67×10^{-6}
250.00	1.50×10^{-8}	1.58×10^{-6}
300.00	8.20×10^{-9}	1.02×10^{-6}
400.00	3.11×10^{-9}	5.08×10^{-7}
500.00	1.45×10^{-9}	2.93×10^{-7}
600.00	7.75×10^{-10}	1.87×10^{-7}
700.00	4.55×10^{-10}	1.27×10^{-7}
800.00	2.86×10^{-10}	9.07×10^{-8}
900.00	1.89×10^{-10}	6.74×10^{-8}
1000.00	1.31×10^{-10}	5.16×10^{-8}
1500.00	3.14×10^{-11}	1.84×10^{-8}
2000.00	1.13×10^{-11}	8.81×10^{-9}
2500.00	5.11×10^{-12}	4.97×10^{-9}
3000.00	2.67×10^{-12}	3.11×10^{-9}

drawn about the most probable value of α when the data were selected to lie in the momentum range in excess of 27.9 GeV/c.

6. Comparison with other results

The present data together with the more recent results obtained by other workers have

been plotted in figure 7. This shows that in the main the spectra produced by the different groups agree within the experimental uncertainties of the results. There are, however, three notable exceptions to this, namely the low-momentum (< 1 GeV/c) differential and integral results produced by Allkofer *et al* (1971), the data from MARS (Ayre *et al* 1971) for momenta below 10 GeV/c for the integral muon intensity and the results of Bateman *et al* in the case of the differential spectrum for momenta less than 20 GeV/c. In order to facilitate the display of other differences between the sea-level spectrum produced at Nottingham and the other results mentioned above the usual technique of plotting the percentage difference of all the data from the proposed spectrum has been adopted and this is shown in figure 8. In this figure error bars are included on a typical set of the data to provide a measure of the uncertainty associated with the experimental points throughout the complete range of momenta covered. Some of the data reported have been taken from best-fit curves which, it should be stated, can only be as accurate as the associated
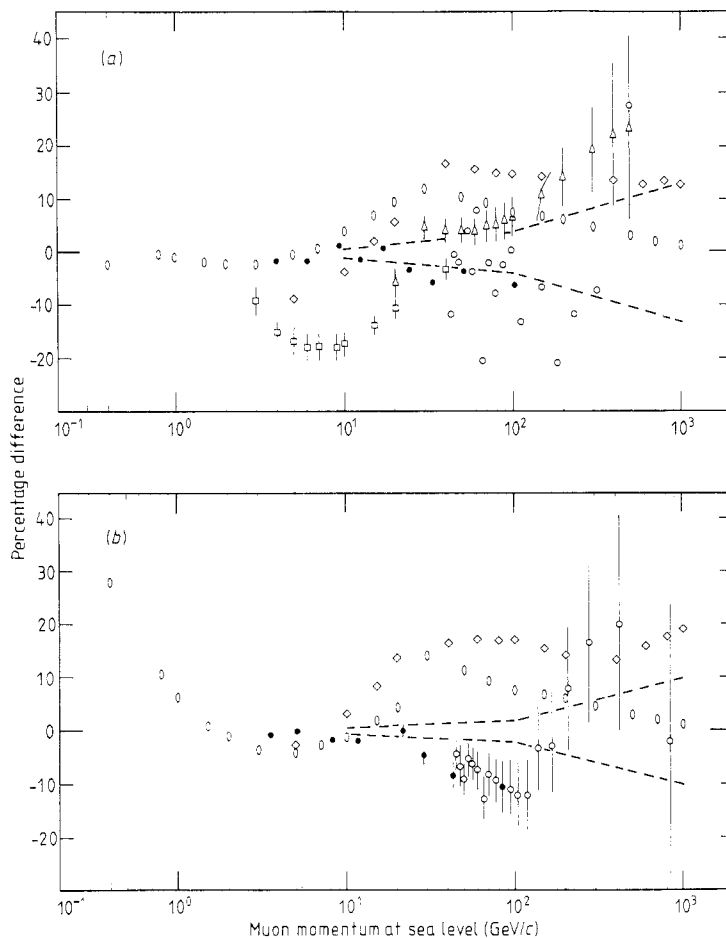

Figure 8. The variation of the percentage difference between the present best-fit spectra and the data obtained by other workers: (*a*) differential; (*b*) integral. – –, Measure of the error on the present best-fit spectra; O, Allkofer *et al* (1971); □, Bateman *et al* (1971); O, Appleton *et al* (1971) for high momentum; ●, Appleton *et al* (1971) for low momentum; ◇, Nandi and Sinha (1972); △, Ayre *et al* (1975).

experimental results; hence the broken lines in figure 8 give an estimate of the effect of experimental errors on the Nottingham best-fit spectrum. The three features mentioned above can be seen clearly in this enhanced plot as well as the possibility of the work of Nandi and Sinha (1972) and Allkofer *et al* (1971) providing slightly higher muon intensities than those produced by the present author within the momentum range from 10 to 100 GeV/c.

7. Conclusions

The present experiment has produced differential and integral muon momentum spectra in the near-vertical direction which cover the range 4 to 2000 GeV/c. These spectra can be described adequately by means of the diffusion model for particle propagation through the atmosphere using a value of -2.73 for the exponent of the primary spectrum together with a K/π ratio at production of 0.087. Such a K/π ratio results in a contribution to the muon integral flux at sea level of about 6% for momenta greater than 5 GeV/c rising to about 20% for momenta greater than 800 GeV/c. However, if consideration is restricted to the high-energy region of the spectra it is also possible to explain the data using a value of -2.60 for the exponent with no contribution from kaon decay. This feature could imply that the assumptions that certain parameters remain constant over the complete range of momentum may not necessarily be correct over the extended range covered by this spectrometer. This interpretation does receive some support from the results obtained using spectrometers which utilised larger solid iron magnets. In these instruments the lower momentum cut-off exceeds that of the present spectrometer and these investigations inevitably result in an exponent in the range -2.60 to -2.67; this is considered further in the appendix. Another possible explanation is that the exponent of the primary spectrum changes from -2.73 to -2.60 at a momentum corresponding to a muon momentum at sea level of about 30 GeV/c. This suggestion provides some tentative support for the proposal made by Liland (1980) which was based on a comparison between experimental results and an analytical solution of the diffusion equations for π mesons and K mesons including an increase with energy of the inelastic nucleon–air-nucleus cross section together with meson production by mesons. Finally the combined results of this investigation and those obtained by Barbouti and Rastin (1983) represent the overall spectrum determined at Nottingham and this covers a momentum range which extends from 0.35 to 3000 GeV/c.

Acknowledgments

Appendix

In order to examine further the effect of the momentum range covered by the instrument on the value obtained for the best-fit exponent the present data were re-analysed with lower momentum cut-offs at 14.59 and 10.16 GeV/c. This showed that the best-fit exponents

corresponding to the selected values of momentum were 2.62 ± 0.02 and 2.65 ± 0.02 for the case of 100% π-meson parentage. The significance levels were 75% and 95%, respectively, indicating that the phenomenological description is increasingly at variance with the experimental results. As previously suggested, this increase in significance level can be interpreted as being associated with the use of an incorrect 'average' for either a constant parameter in the model or the spectral exponent within a region of change. Further, if muon production from K-meson decay was included in the analysis, once again no realistic values of α or γ were obtained since the increase in the magnitude of the exponent could be compensated for by an increase in the contribution from heavy-meson decay.

References

Allkofer O C, Carstensen K and Dau W D 1971 *Phys. Lett.* **36B** 425

Appleton 1 C, Hoque M T and Rastin B C 1971 *Nucl. Phys.* B **26** 365

Ayre C A, Baxendale J M, Hume C J, Nandi B C, Thompson M G and Whalley M R 1975 *J. Phys. G: Nucl. Phys.* **1** 584

Ayre C A, Hamden M A, Hume C J, Nandi B C, Thompson M G, Wells S C, Whalley M R and Wolfendale A W 1971 *J. Phys. A: Gen. Phys.* **4** L89

Barbouti A I and Rastin B C 1983 *J. Phys. G: Nucl. Phys.* **9** 1577

Bateman B J, Cantrell W G, Durda D R, Duller N M, Green P J, Jelinek A V and Nagy T A 1971 *Phys. Lett.* **36B** 144

Bull R M, Coates D W, Nash W F and Rastin B C 1962a *Nuovo Cimento Suppl.* **23** 28

—— 1962b *Nuovo Cimento Suppl.* **23** 39

Bull R M, Nash W F and Rastin B C 1965a *Nuovo Cimento* **40** 348

—— 1965b *Nuovo Cimento* **40** 365

Cousins J, Harrison D J, Hoque M T and Rastin B C 1969 *Proc. 11th Int. Conf. on Cosmic Rays, Budapest* **3** 585

Crookes J N and Rastin B C 1973 *Nucl. Instrum. Methods* **109** 371

Eyges L 1948 *Phys. Rev.* **74** 1534

Harrison D J and Rastin B C 1969 *Nucl. Instrum. Methods* **77** 181

Komori H 1977 *Proc. 15th Int. Conf. on Cosmic Rays, Plovdiv* **6** 26

Lampton M, Margon B and Bowyer S 1976 *Astrophys. J.* **208** 177

Liland A 1980 *Ark. Fys.* (Seminar, Trondheim, Norway) **9** 1

Nandi B C and Sinha M S 1972 *J. Phys. A: Gen. Phys.* **5** 1384

Smith J A and Duller N M 1959 *J. Geophys. Res.* **64** 2297

Rossi B 1952 *High Energy Particles* (Engelwood Cliffs, NJ: Prentice-Hall)

Thompson M G, Thornley R, Whalley M R and Wolfendale A W 1977 *Proc. 15th Int. Conf. on Cosmic Rays, Plovdiv* **6** 21